Prospects of Z' portal dark matter in $U(1)_{L\mu-L\tau}$

Zhen-Wei Wang,[1] Zhi-Long Han,[1,*] Fei Huang,[1,†] Yi Jin,[1,2] and Honglei Li[1,‡]

[1]*School of Physics and Technology, University of Jinan, Jinan, Shandong 250022, China*

[2]*Guangxi Key Laboratory of Nuclear Physics and Nuclear Technology, Guangxi Normal University, Guilin, Guangxi 541004, China*

(Received 19 January 2025; accepted 29 April 2025; published 12 May 2025)

The gauged $U(1)_{L_\mu-L_\tau}$ model is well motivated to explain the muon $g-2$ anomaly and dark matter in previous studies. However, the latest NA64μ experiment has almost excluded all the parameter space for the muon $g-2$, which indicates that the light dark matter benchmark scenarios interpreting muon $g-2$ in previous studies are under significant pressure at present. In light of many recent and future experimental results, we revisit the minimal Z' portal dark matter in $U(1)_{L_\mu-L_\tau}$. Focusing on the phenomenology of dark matter χ, we first explore the viable parameter space for light dark matter under various tight constraints. Around the Z' resonance, we find that there is still a large parameter space for $m_\chi \gtrsim 10$ MeV via thermal freeze-out. On the other hand, the constraints on Z' above the electroweak scale are quite loose, but are less studied for dark matter. We also investigate the heavy dark matter around the TeV scale and corresponding constraints. A large part of the parameter space for dark matter is within the reach of future experiments.

DOI: 10.1103/PhysRevD.111.095017

I. INTRODUCTION

The standard model of particle physics is quite successful at various collider experiments. However, the cosmological and astrophysical observations support the existence of particle dark matter [1], which is absent in the standard model. The weakly interacting massive particle (WIMP), produced via the thermal freeze-out mechanism, can naturally obtain the observed dark matter relic density with electroweak scale couplings [2]. Due to the lack of a positive dark matter signal, the WIMP scenario might be tightly constrained by the collider and direct detection experiments [3]. It should be noted that these tight collider and direct detection limits depend heavily on the WIMP interactions with the quarks [4]. Therefore, one pathway to avoid these limits is assuming the leptophilic dark matter [5–8].

Another hint of new physics beyond the standard model is the 4.2σ excess of the muon $g-2$ [9]. This discrepancy can be resolved by introducing the new gauge boson Z' in the $U(1)_{L_\mu-L_\tau}$ symmetry [10,11], which contributes to the anomalous muon magnetic moment at the one-loop level [12]. The new gauge boson Z' is leptophilic, thus it is also extensively considered as the mediator of dark matter [13–24]. The common origin of muon $g-2$ and light dark matter can be realized with $g' \sim 5\times10^{-4}$ and $m_{Z'} \sim \mathcal{O}(10)$ MeV [25,26]. However, the latest NA64μ experiment has almost excluded all the common parameter space for the muon $g-2$ and light dark matter [27]. So, the benchmark scenarios of light dark matter in previous studies are under significant pressure at present.

Since the new gauge boson Z' does not directly couple to electrons and quarks, the constraints for heavy Z' above the electroweak scale from colliders are relatively loose. For instance, the current LHC search could only probe Z' from the final-state radiation of μ or τ, which is only sensitive when $m_{Z'} < m_Z$ [28,29]. The gauge boson Z' is also lepton flavor dependent, thus it can explain the deviation of lepton universality in beauty-quark decays with heavy dark matter [30–34]. Recently, the TeV energy scale muon collider has been proposed [35,36], which is promising to probe the muonphilic Z' above the electroweak scale [37–40].

In light of recent and upcoming experiments, we revisit the Z' portal dark matter in the $U(1)_{L_\mu-L_\tau}$ symmetry. We focus on the phenomenology of dark matter, meanwhile excess of muon $g-2$ might be resolved by other new physics [12,41]. The simplest scenario of Dirac dark matter χ with the $U(1)_{L_\mu-L_\tau}$ charge $Q_\chi = 1$ is illustrated in this paper. Other possible assignment of Q_χ and scalar dark matter can be found in Refs. [42–47].

This paper is organized as follows. In Sec. II, we briefly review the Z' portal dark matter in $U(1)_{L_\mu-L_\tau}$ and various experimental constraints. The phenomenology of dark

*Contact author: sps_hanzl@ujn.edu.cn
†Contact author: sps_huangf@ujn.edu.cn
‡Contact author: sps_lihl@ujn.edu.cn

matter is discussed in Sec. III. Finally, conclusions are presented in Sec. IV.

II. THE MODEL

For the simplest Dirac dark matter with the $U(1)_{L_\mu - L_\tau}$ charge $Q_\chi = 1$, the relevant interactions of the new gauge boson Z' are [26]

$$\mathcal{L} \supset g'(\bar{\mu}\gamma^\mu\mu - \bar{\tau}\gamma^\mu\tau + \bar{\nu}_\mu\gamma^\mu P_L\nu_\mu - \bar{\nu}_\tau\gamma^\mu P_L\nu_\tau + \bar{\chi}\gamma^\mu\chi)Z'_\mu, \tag{1}$$

where g' is the new gauge coupling. The mass of the new gauge boson arises from the spontaneous breaking of $U(1)_{L_\mu - L_\tau}$ symmetry by the scalar singlet ϕ with $U(1)_{L_\mu - L_\tau}$ charge $+1$, i.e., $m_{Z'} = g' v_\phi$, where v_ϕ is the vacuum expectation value of ϕ. For simplicity, the direct kinetic mixing term between the new and hypercharge gauge field is assumed to be zero. However, radiative corrections at the one-loop level still induce finite mixing as

$$\mathcal{L} \supset -\frac{\varepsilon}{2} F_{\mu\nu} F'^{\mu\nu}, \tag{2}$$

where $F_{\mu\nu}$ and $F'_{\mu\nu}$ are the field strength for photon and Z', respectively. The mixing parameter is calculated as [48]

$$\varepsilon = -\frac{e g'}{12\pi^2} \ln\frac{m_\tau^2}{m_\mu^2} \simeq -\frac{g'}{70}. \tag{3}$$

The dominant partial decay widths of Z' are

$$\Gamma_{Z' \to f\bar{f}} = \frac{k_f g'^2 m_{Z'}}{12\pi}\left(1 + \frac{2m_f^2}{m_{Z'}^2}\right)\sqrt{1 - \frac{4m_f^2}{m_{Z'}^2}}, \tag{4}$$

where $k_f = 1$ for $f = \mu, \tau, \chi$ and $k_f = 1/2$ for $f = \nu_\mu, \nu_\tau$. Through kinetic mixing, the partial width of $Z' \to e^+e^-$ is given by

$$\Gamma_{Z' \to e^+e^-} = \frac{(\varepsilon e)^2 m_{Z'}}{12\pi}\left(1 + \frac{2m_e^2}{m_{Z'}^2}\right)\sqrt{1 - \frac{4m_e^2}{m_{Z'}^2}}, \tag{5}$$

which is typically suppressed by the mixing [49].

Contribution to the muon magnetic moment of Z' is at the one-loop level, which is calculated as [11]

$$\Delta a_\mu = \frac{g'^2}{4\pi^2}\int_0^1 dx \frac{m_\mu^2 x(1-x)^2}{m_\mu^2(1-x)^2 + m_{Z'}^2 x^2}. \tag{6}$$

To explain the anomaly $\Delta a_\mu = (251 \pm 59) \times 10^{-11}$ [9], $g' \sim 5 \times 10^{-4}$ with $m_{Z'} \sim \mathcal{O}(10)$ MeV is required, which is now stringently constrained by the latest NA64μ experiment [27].

A. Constraints

Decays of gauge boson Z' will heat the neutrino population and delay the process of neutrino decoupling, which increases the effective number of neutrino species $N_{\rm eff}$ [48]. The precise measurement of the Planck result $N_{\rm eff} = 2.99 \pm 0.17$ [50] is consistent with the standard model prediction $N_{\rm eff}^{\rm SM} = 3.044$ [51,52], which disfavors the light Z' region with $m_{Z'} \lesssim 10$ MeV [48]. In Fig. 1, we show the $N_{\rm eff}^{\rm SM}$ excluded region with the color blue.

The gauge boson Z' could affect the evolution of white dwarfs (WDs) by enhancing the plasmon decay into neutrinos. Around $m_{Z'} \sim 10$ MeV, the recent analysis in Ref. [53] shows that the constraint from WD cooling is more stringent than the $\nu - e$ scattering by BOREXINO [61]. The WD cooling excluded region is marked as yellow in Fig. 1.

The gauge boson Z' also contributes to the neutrino trident production via the inelastic neutrino-nucleus scattering $\nu_\mu N \to \nu_\mu N \mu^+\mu^-$ [55]. The CCFR experiment has measured the normalized cross section $\sigma/\sigma_{\rm SM} = 0.82 \pm 0.28$ [62], which has excluded the heavy Z' region with $m_{Z'} \gtrsim 0.3$ GeV for the muon anomalous magnetic moment. The gray region in Fig. 1 is not allowed by the CCFR experiment.

For light gauge bosons below the dimuon threshold, the invisible $Z' \to \bar{\nu}\nu$ is the dominant decay mode [49]. The gauge boson Z' could be tested through the bremsstrahlung process, $\mu N \to \mu N Z', Z' \to \bar{\nu}\nu$, by the high-energy muon scattering off nucleus N, which leads to the signature of missing momentum in the final state. The region with $g' \gtrsim 6 \times 10^{-4}$ and $m_{Z'} \sim \mathcal{O}(10)$ MeV is now excluded by the NA64μ experiment [27], which corresponds to the purple region in Fig. 1. In the future, the NA64 [63] and LDMX [57] (the dashed purple line in Fig. 1) experiments are expected to probe $g' \gtrsim 10^{-5}$ for $m_{Z'} \lesssim 1$ GeV. Meanwhile, the future SHiP experiment (the dashed cyan line in Fig. 1) could probe $g' \gtrsim 10^{-6}$ for $m_{Z'} \sim \mathcal{O}(10)$ MeV [56].

Above the dimuon threshold, $Z' \to \mu^+\mu^-$ becomes the promising channel. The searches of the process $e^+e^- \to \mu^+\mu^- Z', Z' \to \mu^+\mu^-$ at *BABAR* [54] and Belle-II [64] have excluded $g' \gtrsim 10^{-3}$ for Z' mass in the range of 0.212–10 GeV, which is the orange region in Fig. 1. Through the muon bremsstrahlung process $\mu\,\mathrm{Au} \to \mu\,\mathrm{Au}\,Z'$, the proposed MuSIC experiment (the dashed red line in Fig. 1) could probe the parameter space with $g' \gtrsim 10^{-7}$ for $m_{Z'} \in [0.212, 20]$ GeV [58]. The future Beam Dump experiment (the dashed green line in Fig. 1) could further reach $g' \sim 4 \times 10^{-8}$ [59]. At the Hadron Collider, searches for Z' have been performed in the process as $pp \to Z^{(*)} \to Z'\mu^+\mu^- \to \mu^+\mu^-\mu^+\mu^-$ [28] and $pp \to W^{\pm(*)} \to Z'\mu^\pm\nu \to \mu^+\mu^-\mu^\pm\nu$ [29], which have excluded $g' \gtrsim 0.003$ in the Z' mass range of 5–81 GeV. The excluded region by the current ATLAS experiment is the red area in Fig. 1. In the future, the FCC-ee collider (the dashed brown line in Fig. 1) could push this limit down to $g' \gtrsim 10^{-4}$ [60]. Meanwhile,

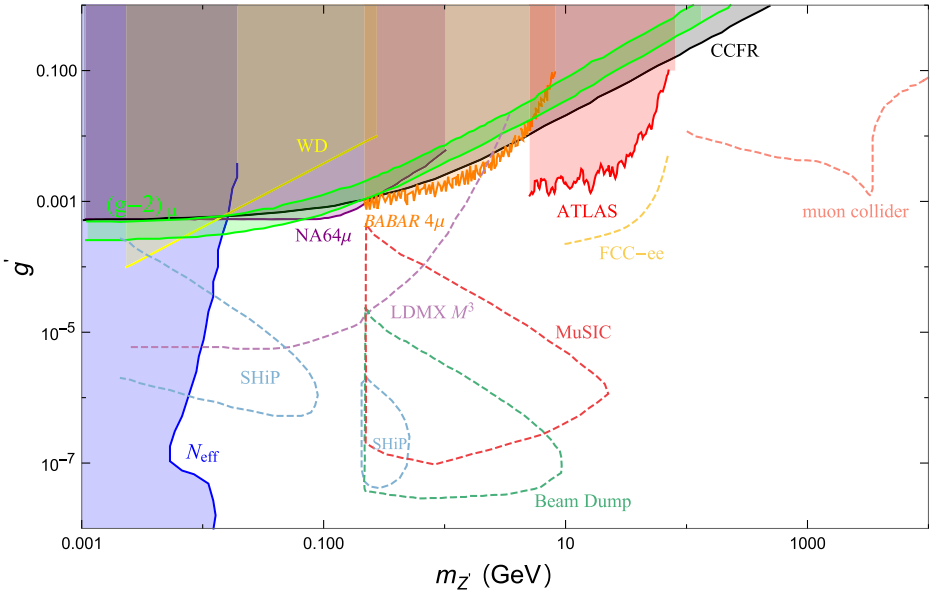

FIG. 1. Present and future constraints on the gauged $U(1)_{L_\mu - L_\tau}$. The green band is the $(g-2)_\mu$ favored region. The blue, yellow, purple, orange, red, and gray regions are excluded by $N_{\rm eff}$ [48], WD cooling [53], NA64μ [27], *BABAR* [54], ATLAS [29], and CCFR [55], respectively. The dashed cyan, purple, red, green, brown, and pink lines are the future reach of SHiP [56], LDMX [57], MuSIC [58], Beam Dump [59], FCC-ee [60], and the muon collider [37].

the muon collider (the dashed pink line in Fig. 1) could probe a large parameter space for Z' above the electroweak scale [37,38].

In Fig. 1, we summarize the latest and future constraints on gauged $U(1)_{L_\mu - L_\tau}$. Light Z' below 10 MeV is now excluded by $N_{\rm eff}$. The current experiments typically exclude $g' \gtrsim 10^{-3}$ in the range of 10 MeV–100 GeV. For $m_{Z'}$ below 0.2 GeV, a large portion of the parameter space could be covered by the LDMX [57] and SHiP experiments [56]. For $m_{Z'}$ in the range of 0.2–20 GeV, the MuSIC [58] and Beam Dump experiments [59] would test $g' \gtrsim 4 \times 10^{-8}$. For $m_{Z'} \gtrsim \mathcal{O}(10)$ GeV, FCC-ee [60] is the ideal machine to probe the new gauge boson. Above the electroweak scale, the future muon collider [37,38] could reveal most regions with $g' \gtrsim 10^{-3}$.

At the muon collider, the dark matter can be generated via the new gauge boson Z'. One promising channel is the monophoton signature $\mu^+\mu^- \to \gamma Z' \to \gamma\bar{\chi}\chi \to \gamma \not{E}_T$ [65], which also has new physics contribution from the process $\mu^+\mu^- \to \gamma Z' \to \gamma\bar{\nu}\nu$ in this paper. Therefore, the contribution from dark matter to the monophoton signature can be extracted by the precise measurement of the invisible branching ratio of Z'.

III. DARK MATTER

A. Relic density

In this paper, we consider dark matter produced through the freeze-out mechanism. The evolution of the dark matter relic density is then determined by the Boltzmann equation [26]

$$\frac{dn}{dt} + 3Hn = -\frac{\langle\sigma v\rangle}{2}(n^2 - n_{\rm eq}^2), \tag{7}$$

where H is the Hubble parameter, $n = n_\chi + n_{\bar{\chi}}$ is the total number density of dark matter, and $n_{\rm eq}$ is the equilibrium number density.

If kinematically allowed, the dark matter χ could annihilate via the s-channel processes $\chi\bar{\chi} \to f\bar{f}(f = \mu, \tau, \nu_\mu, \nu_\tau)$ and the t-channel process $\chi\bar{\chi} \to Z'Z'$. The corresponding thermally averaged annihilation cross sections are

$$\langle\sigma v\rangle_{\chi\bar{\chi}\to f\bar{f}} \simeq \frac{\kappa_f g'^4}{2\pi m_\chi} \frac{(2m_\chi^2 + m_f^2)(m_\chi^2 - m_f^2)^{1/2}}{(4m_\chi^2 - m_{Z'}^2)^2 + m_{Z'}^2\Gamma_{Z'}^2}, \tag{8}$$

$$\langle\sigma v\rangle_{\chi\bar{\chi}\to Z'Z'} \simeq \frac{g'^4}{4\pi m_\chi} \frac{(m_\chi^2 - m_{Z'}^2)^{3/2}}{(2m_\chi^2 - m_{Z'}^2)^2}, \tag{9}$$

where $\Gamma_{Z'}$ is the total decay width of Z'. To properly calculate the annihilation cross section near the Z' pole [66], we use micrOMEGAs [67] to obtain the numerical results of the relic density.

In Fig. 2, we show the required values of g' and $m_{Z'}$ to generate the observed dark matter relic density $\Omega_\chi h^2 = 0.12 \pm 0.001$ [50] for three benchmark scenarios with masses of $m_\chi = 0.05$, 5, and 500 GeV. With stringent constraints, the sub-GeV and GeV scale dark matter can only satisfy relic density near the Z' resonance. The future LDMX [57] (the dashed purple line in Fig. 2) and FCC-ee experiments [60] (the dashed brown line in Fig. 2) would probe such scenarios. Meanwhile, the SHiP [56] (the

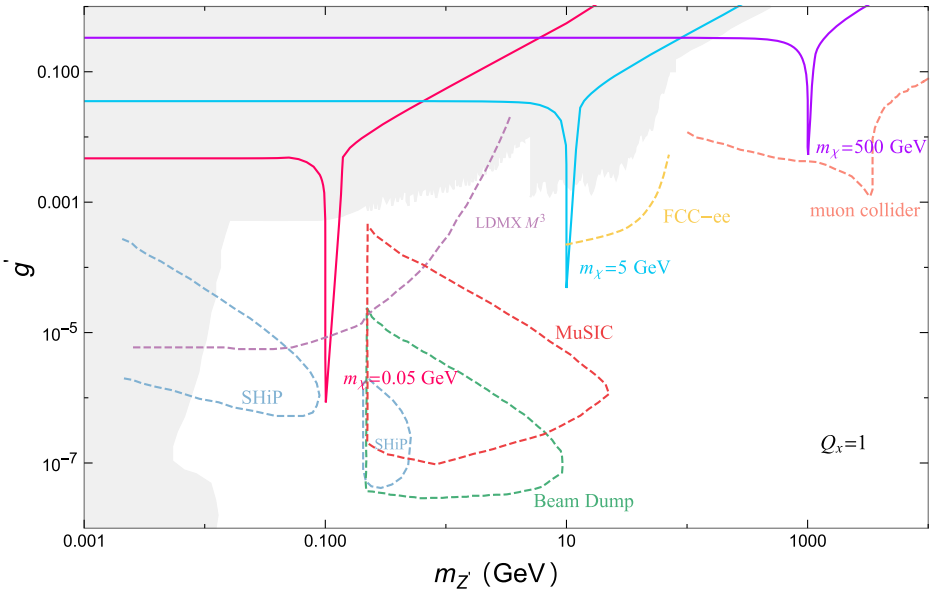

FIG. 2. Required values of g' and $m_{Z'}$ to generate the observed dark matter relic density. The red, blue, and purple lines correspond to dark matter mass $m_\chi = 0.05$, 5, and 500 GeV, respectively. The gray region is excluded by current searches. Other labels are the same as in Fig. 1.

dashed cyan line in Fig. 2) and MuSIC experiments [58] (the dashed red line in Fig. 2) are expected to test certain resonance regions. For dark matter mass larger than the electroweak scale, the $\chi\bar{\chi} \to Z'Z'$ channel could also have a significant contribution to relic density. It is also clear that the muon collider [37,38] (the dashed pink line in Fig. 2) is able to cover the whole Z' resonance region around the TeV scale.

B. Direct detection

Although the dark matter (DM) χ does not couple directly to quarks or electrons, the loop-induced kinetic mixing term in Eq. (2) contributes to the elastic DM-nucleon scattering. The spin-independent DM-nucleon scattering cross section is calculated as

$$\sigma_{\chi N} = \frac{\mu_N^2}{\pi} \frac{Z^2 g'^2 \varepsilon^2 e^2}{A^2 m_{Z'}^4}, \tag{10}$$

where $\mu_N = m_\chi m_N/(m_\chi + m_N)$ is the reduced DM-nucleon mass. A and Z are the mass and atomic number of the nucleus.

Currently, the CRESST-III experiment [68] (the orange line in Fig. 3) has excluded $\sigma_{\chi N} \gtrsim 10^{-38}$ cm^2 for sub-GeV DM. The DarkSide-50 [69] (the yellow line in Fig. 3) could exclude $\sigma_{\chi N} \gtrsim 10^{-43}$ cm^2 for GeV DM. In the mass range of 6–10 GeV, XENONnT [70] (the dark green line in Fig. 3) has set the most stringent limit. Above 10 GeV, LZ (the light green line in Fig. 3) could exclude $\sigma_{\chi N} \gtrsim 2 \times 10^{-48}$ cm^2. In the near future, the DarkSide-20k [71] (the dashed green line in Fig. 3) and DARWIN experiments [72] (the dashed red line in Fig. 3) could push the limit down to the level of neutrino fog [73].

In Fig. 3, we show the predicted DM-nucleon scattering cross section for the benchmark scenario with $m_{Z'} = 0.1$, 10, 1000 GeV, where correct relic density $\Omega_\chi h^2 = 0.12$ and $g' < 1$ are further required. When $m_\chi < m_{Z'}$, we approximately need $g' \sim \mathcal{O}(0.01)$ for $m_{Z'} = 0.1$ GeV, $g' \gtrsim 0.01$ for $m_{Z'} = 10$ GeV, and $g' \sim \mathcal{O}(0.1)$ for $m_{Z'} = 1000$ GeV. Within the resonance region, the relic density required value of g' is much smaller, which could be down to about $g' \sim 10^{-5} \times (m_{Z'}/\text{GeV})$. Meanwhile, we roughly have $g' \sim 0.02 \times \sqrt{m_\chi/\text{GeV}}$ when dark matter χ is heavier than gauge boson Z'.

Due to too small recoil energy, the DM-nucleon experiments lose the sensitivity for light DM $m_\chi \ll m_N$. So, there is no DM-nucleon limit for $m_\chi \lesssim 0.1$ GeV. Although (sub-) GeV DM in the nonresonance region could lead to a smaller scattering cross section than the current experimental limit, the direct searches for Z' already disfavor such scenario with correct relic density. The predicted scattering cross section in the resonance region could be as small as 10^{-53} cm^2, which is far beyond the future experimental reach. For the canonical electroweak scale DM, it is obvious that the current LZ [74] has excluded the nonresonance region. As there is no other experimental limit in this region at present, the direct detection experiments set the most stringent constraint. A positive signature is also expected in the future DARWIN operation [72].

For light dark matter below 1 GeV, the constraints from DM-electron scattering would be more stringent. The DM-electron scattering cross section is calculated as

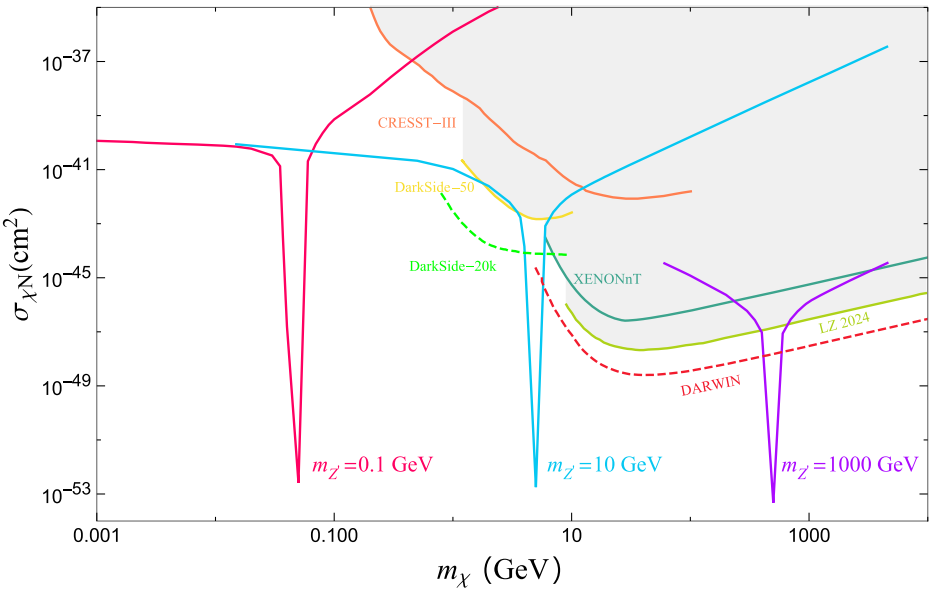

FIG. 3. Predicted DM-nucleon scattering cross section and various experimental limits. The red, blue, and purple lines are the benchmark scenario with $m_{Z'} = 0.1$, 10, and 1000 GeV, respectively. The orange, yellow, dark green, and light green solid lines are the limits of CRESST-III [68], DarkSide-50 [69], XENONnT [70], and LZ [74]. The green and red dashed lines are the future reach of DarkSide-20k [71] and DARWIN [72].

$$\sigma_{\chi e} = \frac{\mu_e^2}{\pi} \frac{g'^2 \varepsilon^2 e^2}{(m_{Z'}^2 + \alpha^2 m_e^2)^2}, \tag{11}$$

where $\mu_e = m_\chi m_e/(m_\chi + m_e)$ is the reduced DM-electron mass, and α is the fine structure constant.

Below 10 MeV, SENSEI [75,76] (the green line in Fig. 4) could exclude $\sigma_{\chi e} \gtrsim 10^{-36}$ cm^2. In the mass range of 10–30 MeV, PandaX-II [77] (the orange line in Fig. 4) gives the most stringent limit. Above 30 MeV, XENON1T [78] (the dark blue line in Fig. 4) could exclude $\sigma_{\chi e} \gtrsim 10^{-40}$ cm^2. In the future, SuperCDMS-G2+ [79] (the dashed purple line in Fig. 4) would probe $\sigma_{\chi e} \gtrsim 10^{-42}$ cm^2 for sub-GeV DM.

In Fig. 4, we depict the predicted DM-electron scattering cross section with the correct relic density. Explicit values

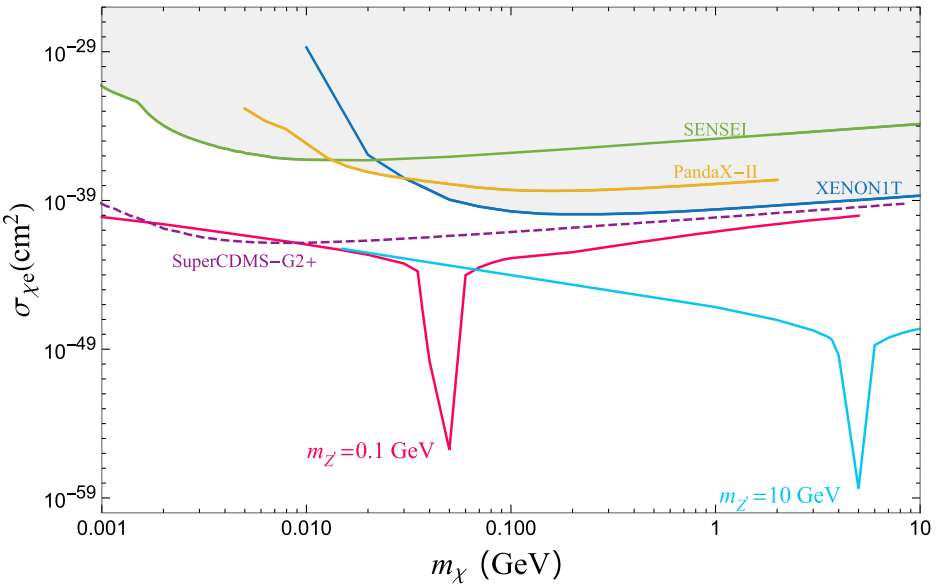

FIG. 4. Predicted DM-electron scattering cross section and various experimental limits. The red and blue lines are the benchmark scenario with $m_{Z'} = 0.1$ and 10 GeV. The green, orange, and dark blue lines are the limits of SENSEI [75,76], PandaX-II [77], and XENON1T [78], respectively. The purple dashed line is the future limit from SuperCDMS-G2+ [79].

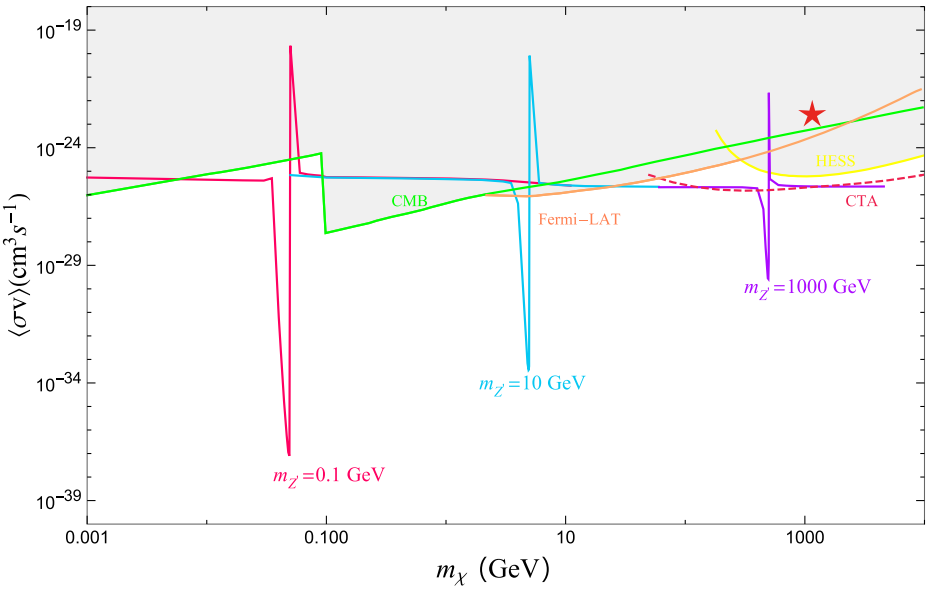

FIG. 5. Predicted annihilation cross section and various constraints. The red, blue, and purple lines are the benchmark scenario with $m_{Z'} = 0.1$,10, and 1000 GeV, respectively. The green, orange, and yellow lines are the current limits from CMB [84], Fermi-LAT [85], and HESS [86]. The red dashed line is the future reach of the CTA experiment [87]. The red star could interpret the AMS-02 observed positron excess [88].

of g' are the same as in Fig. 3. Suppressed by the loop-induced kinetic mixing, we find that the theoretical predicted value is far smaller than the current experimental limits. In principle, the future SuperCDMS-G2+ experiment [79] could probe the nonresonance region around $m_\chi \sim \mathcal{O}$ (MeV). However, this region has been excluded by direct searches for Z'. Therefore, no positive signal is expected in the near future DM-electron experiments.

C. Indirect detection

As shown in Figs. 2 and 3, the combined results of relic density and direct detection experiments favor the Z' resonance region. Considering the relatively loose constraints on DM annihilation into neutrinos [80], we also neglect the contribution from neutrino final states for simplicity, which could have a sizable impact for $m_\chi >$ 100 GeV [81] in the following discussion. Therefore, we only consider the s-channel processes $\chi\bar{\chi} \to \ell^+\ell^-$ for the indirect detection constraints.

Annihilation of DM into charged fermions can inject energy to increase the ionization fraction during the era of recombination, which modifies the spectrum of cosmic microwave background (CMB) anisotropy [82]. Planck collaboration has set a stringent limit on the annihilation parameter [50],

$$p_{\mathrm{ann}} = \sum_{\ell=e,\mu,\tau} \frac{1}{2} f^{\ell}_{\mathrm{eff}} \cdot \mathrm{FR}_\ell \frac{\langle\sigma v\rangle}{m_\chi} < 3.5 \times 10^{-28}\ \mathrm{cm}^3\,\mathrm{s}^{-1}\,\mathrm{GeV}^{-1}, \tag{12}$$

where f^{ℓ}_{eff} is the efficiency factor of the deposited energy for lepton ℓ [83], and FR_ℓ is the fraction of individual channel $\chi\bar{\chi} \to \ell^+\ell^-$ to the total DM annihilation cross section $\langle\sigma v\rangle$. Different from previous results for individual channels of e^+e^-, $\mu^+\mu^-$, and $\tau^+\tau^-$ [84], we obtain the CMB constraint on the total annihilation cross section $\langle\sigma v\rangle$ to compare with other limits, which is the green line in Fig. 5. In this model, the fraction of $\chi\bar{\chi} \to e^+e^-$ is suppressed by the kinetic mixing [26]. Therefore, the CMB constraint is relaxed when $m_\chi < m_\mu$ [25].

The annihilation of DM could lead to high-energy photons, which can be tested by Fermi-LAT [85] and HESS [86] experiments. The Fermi-LAT results (the orange line in Fig. 5) could exclude 2 GeV $\lesssim m_\chi \lesssim$ 100 GeV for DM only annihilating into the $\tau^+\tau^-$ final sate with the typical thermal cross section $\sim 2 \times 10^{-26}$ cm^3 s^{-1} [85]. Around the TeV scale, the HESS experiment (the yellow line in Fig. 5) sets the most stringent limit, which could exclude $\langle\sigma v\rangle \gtrsim 2 \times 10^{-26}$ cm^3 s^{-1} in the pure $\tau^+\tau^-$ final state [86]. In the future, the CTA experiment (the dashed red line in Fig. 5) would cover a large parameter space for DM above 100 GeV [87].

In this model, the theoretical predicted differential photon flux is calculated as

$$\frac{d\Phi_\gamma}{dE_\gamma} = \frac{\langle\sigma v\rangle}{8\pi m_\chi^2} \sum_{\ell=\mu,\tau} \mathrm{FR}_\ell \frac{dN^{\ell}_\gamma}{dE_\gamma} \cdot J_{\mathrm{ann}}, \tag{13}$$

where E_γ is the energy of the photon, $dN^{\ell}_\gamma/dE_\gamma$ is the differential photon spectrum from lepton final states $\ell^+\ell^-$,

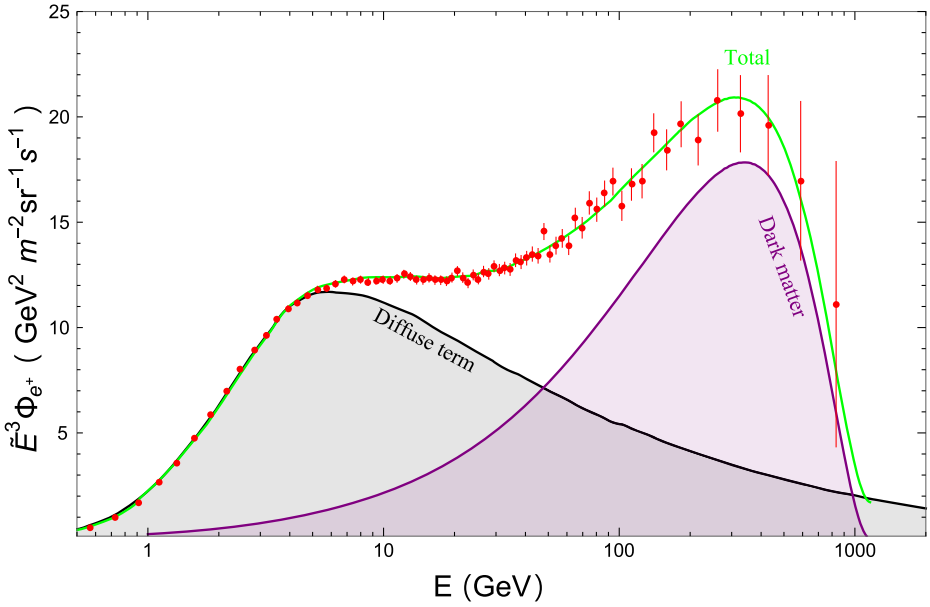

FIG. 6. The flux of the cosmic positron measured by AMS-02 (red samples) [88] and the theoretical total flux from dark matter annihilation (green line). The diffuse term contribution is the black line, and the source term from dark matter is the purple line. Here, $m_{Z'}/2 \simeq m_\chi = 1160$ GeV.

and $J_{\rm ann}$ is the astrophysical J factor [85]. For $m_\chi \gtrsim 10$ GeV, the fraction is $\mathrm{FR}_\mu \simeq \mathrm{FR}_\tau \simeq 1/3$. Because the fraction of the e^+e^- final state is tiny for $U(1)_{L_\mu - L_\tau}$ DM in the indirect experiment sensitive region $m_\chi > 2$ GeV, the contribution from the e^+e^- final sate is neglected. From the results of Fermi-LAT [85], it is obvious that the constraint from the individual $\tau^+\tau^-$ final state is much more stringent than that from the individual $\mu^+\mu^-$ final state. Therefore, the photon flux in this model is dominant by the $\tau^+\tau^-$ final sate with equal fraction $\mathrm{FR}_\mu \simeq \mathrm{FR}_\tau \simeq 1/3$. Considering potential large astrophysical uncertainties, we then roughly estimate the indirect constraints by rescaling the experimental results as $\langle\sigma v\rangle \simeq \langle\sigma v\rangle_{\tau^+\tau^-}/\mathrm{FR}_\tau \approx 3\langle\sigma v\rangle_{\tau^+\tau^-}$, where $\langle\sigma v\rangle_{\tau^+\tau^-}$ is the indirect constraint for the individual $\tau^+\tau^-$ channel. More tedious but precise results can be obtained by performing the likelihood analysis [89].

Figure 5 shows the predicted annihilation cross section with correct relic density and corresponding constraints. Explicit values of g' are the same as in Fig. 3. In the nonresonance region, the typical annihilation cross section is $(2 \sim 3) \times 10^{-26}$ cm^3 s^{-1}. Current indirect detection then excludes the mass range of 0.1–100 GeV. At the TeV scale, the HESS limit [86] is slightly larger than the thermal target of the nonresonance scenario. In the future, the CTA experiment [87] is hopeful to probe such a region. In the resonance region, the annihilation cross section heavily depends on the mass relation between Z' and χ, due to different DM velocities at the time of freeze-out $v_f \sim \mathcal{O}(0.1)$ and at present $v_0 \sim \mathcal{O}(0.001)$. When $m_\chi \simeq m_{Z'}/2$ is at the Z' pole, the annihilation cross section can be greatly enhanced at present [90], which is disfavored by current experimental limits. On the other hand, when the pole condition $m_\chi \simeq m_{Z'}/(2\sqrt{1+v_f^2/\sqrt{2}}) \sim 0.49 m_{Z'}$ is satisfied at freeze-out, the present cross section is suppressed [91]. Therefore, m_χ slightly below the Z' pole can easily avoid the tight constraints from indirect detection.

Besides photons, indirect detection experiments also measure other cosmic rays, such as positrons. AMS-02 collaboration has reported an excess of positron flux with a peak of around 300 GeV [88], which might be explained by dark matter in $U(1)_{L_\mu - L_\tau}$ [92]. In Fig. 6, we show the benchmark point with $m_{Z'}/2 \simeq m_\chi = 1160$ GeV that could generate the observed positron excess. The induced positron flux from DM annihilation is obtained with micrOMEGAs [67], where both the $\mu^+\mu^-$ and $\tau^+\tau^-$ final states are considered. It should be noted that the positron excess required annihilation cross section is about $\langle\sigma v\rangle \simeq 4 \times 10^{-23}$ cm^3 s^{-1}. Although such large annihilation can be realized at the Z' pole, all the indirect detection limits disfavor such a large annihilation cross section, as shown in Fig. 5. By fine-tuning the mass relation of m_χ and $m_{Z'}$, the indirect detection limits on DM for positron excess might be relaxed due to velocity-dependent annihilation [93]. Anyway, the positron excess requires TeV scale Z' with $g' \sim \mathcal{O}(0.01)$, which is within the reach of the future muon collider [37,38].

D. Combined result

The experimental searches for new gauge boson Z' have set stringent constraints for light Z' below about 100 GeV. Meanwhile, the direct and indirect detection experiments

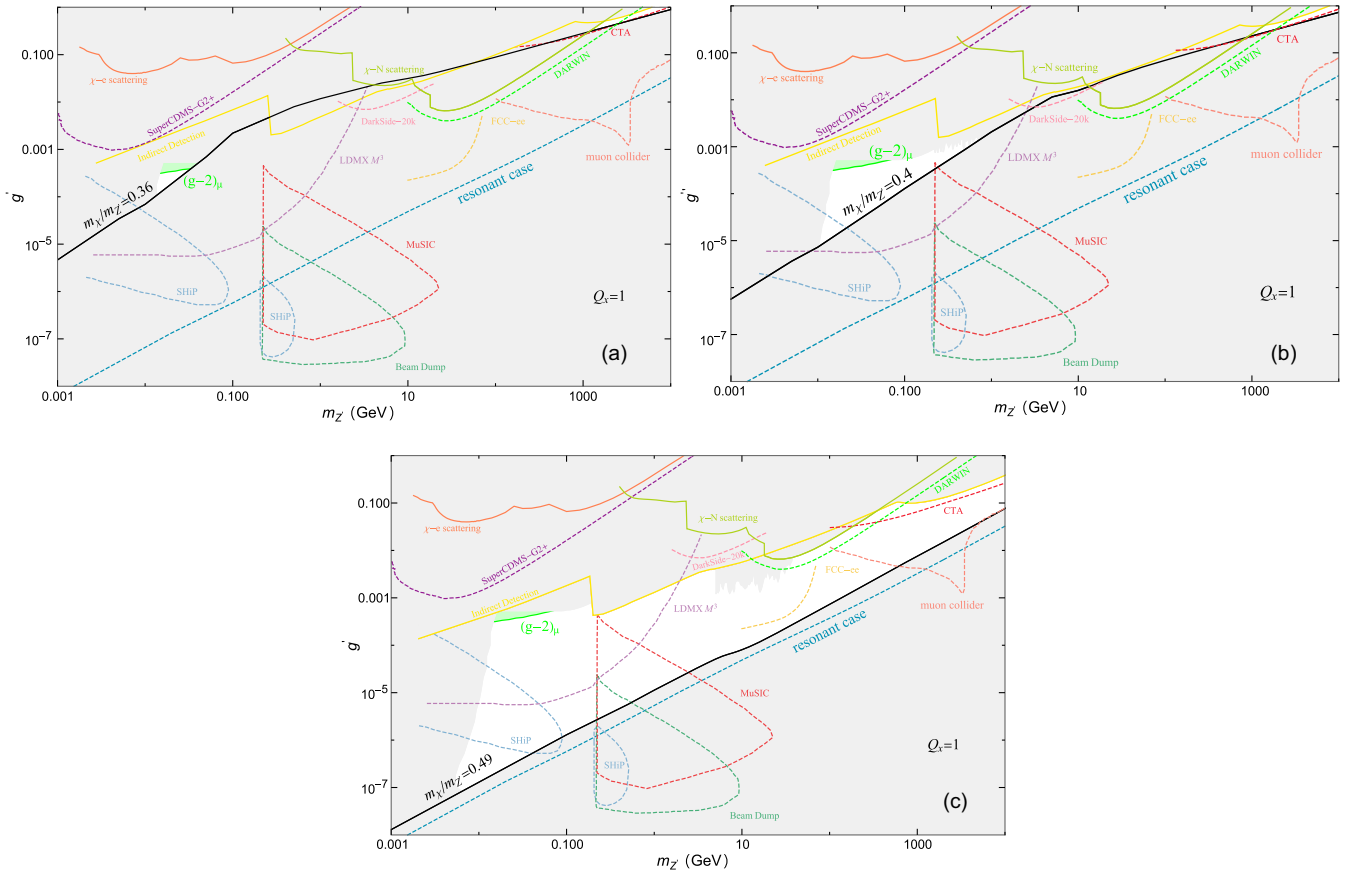

FIG. 7. The combined parameter space of benchmark scenario $m_\chi/m_{Z'} = 0.36$ in panel (a), $m_\chi/m_{Z'} = 0.4$ in panel (b), and $m_\chi/m_{Z'} = 0.49$ in panel (c). The green region could interpret the $(g-2)_\mu$ anomaly under current limits. The orange, green, and yellow solid lines are the combined limits from $\chi - e$ scattering, $\chi - N$ scattering, and indirect detection at present, respectively. The black lines are the required values of g' and $m_{Z'}$ for correct relic density, below which the DM relic density is overabundant. The dashed dark blue lines are the minimum required value of g' for the resonance case $m_{Z'} \simeq 2m_\chi$ with $Q_\chi = 1$. Other labels are the same as in Fig. 1.

on dark matter mainly constrain heavy DM above 10 GeV. In this section, we combine all the relevant constraints at present and in the future. As the conventional benchmark scenario with $m_\chi/m_{Z'} = 1/3$ is already disfavored by various experiments [25], we consider three new benchmark scenarios in this paper: one is $m_\chi/m_\chi = 0.36$ for $(g-2)_\mu$ anomaly, one is $m_\chi/m_{Z'} = 0.4$, and the other one is $m_\chi/m_{Z'} = 0.49$. The results are shown in Fig. 7.

It is obvious that the current DM-electron scattering experiments can only probe $g' \gtrsim 0.1$ and $m_{Z'} \lesssim 1$ GeV. Although the future SuperCDMS-G2+ [79] could test $g' \gtrsim 0.001$, such region is already excluded by current direct searches of Z'. Therefore, no positive signature is expected in the future DM-electron experiments for the Z' portal DM $U(1)_{L_\mu - L_\tau}$. On the other hand, the limits from DM-nucleon scattering and indirect detection become the most stringent constraints for $m_{Z'} \gtrsim 100$ GeV, as there is no direct search of Z' in such a region. In the future, the muon collider [37,38] would cover most of the parameter space for correct relic density.

One interesting scenario is explaining the $(g-2)_\mu$ and dark matter relic density simultaneously. Under current stringent constraints, we find that this still can be realized with $m_\chi/m_{Z'} \simeq 0.36$. The viable region satisfies $g' \sim 4 \times 10^{-4}$ with $m_{Z'} \sim \mathcal{O}(0.01)$ GeV, which is within the reach of future NA64 [63] and LDMX [57] experiments.

For the benchmark scenario with $m_\chi/m_{Z'} = 0.4$, the viable region is separated into two parts. The light sub-GeV region is totally within the reach of LDMX [57], and could be further confirmed by SHiP for $m_{Z'} \sim \mathcal{O}(0.01)$ GeV. However, the MuSIC [58] and Beam Dump experiments [59] can hardly probe such a large g' required by relic density. The GeV to TeV mass range set by relic density is now excluded by direct search of Z' and direct detection. Around $m_{Z'} \approx 2$ TeV, the predicted DM-nucleon scattering cross section can be tested at DARWIN [72], and the indirect detection CTA experiment [87] is also capable of probing such a region. The typical relic density required gauge coupling $g' \sim \mathcal{O}(0.1)$ can be easily confirmed at the muon collider [37,38]. Therefore, this region with

$m_{Z'} \approx 2$ TeV is the most promising one in the forthcoming experiments.

Different from the previous benchmark scenario with $m_\chi/m_{Z'} = 0.4$, the benchmark scenario with $m_\chi/m_{Z'} = 0.49$ is close to the Z' resonance. As the annihilation cross section at the time of freeze-out is enhanced by the Breit-Wigner propagator, the relic density required gauge coupling for $m_\chi/m_{Z'} = 0.49$ is typically 2 orders of magnitude smaller than that for $m_\chi/m_{Z'} = 0.4$. In this way, we find that $m_{Z'} \gtrsim 0.01$ GeV is all viable at present. Although the suppressed gauge coupling makes this scenario satisfy all constraints, it also makes this scenario hard to detect. For instance, all the dark matter detection experiments cannot probe this scenario. The SHiP experiment [56] could probe $m_{Z'} \simeq 0.08$ GeV, while the MuSIC experiment [58] could test Z' in the mass range of 0.2–2 GeV. The TeV muon collider [37,38] would explore the region with $m_{Z'} \gtrsim 600$ GeV. To cover the parameter space around 100 GeV, a muon collider operating at the electroweak scale is strongly encouraged.

IV. CONCLUSION

Although the new gauge boson Z' in $U(1)_{L_\mu - L_\tau}$ is extensively studied as the interpretation of muon $g-2$, the latest experimental result does not favor the corresponding parameter space. In this paper, we revisited the minimal Z' portal dark matter in the gauged $U(1)_{L_\mu - L_\tau}$ model, which introduces a singlet Dirac fermion χ with the $U(1)_{L_\mu - L_\tau}$ charge $Q_\chi = 1$ as the dark matter candidate.

The combined analysis showed that light dark matter suffers stringent constraints from searches for Z'. For example, $m_{Z'}$ less than 10 MeV was excluded by the effective number of neutrino species $N_{\rm eff}$. The new gauge coupling g' should be smaller than 0.001 to satisfy current limits. On the other hand, the direct and indirect detection experiments set the most strict constraints for the heavy dark matter. To satisfy current experimental limits, dark matter near the Z' resonance region is favored.

In the $U(1)_{L_\mu - L_\tau}$ model, the coupling of Z' to the electron was suppressed by the kinetic mixing term. Under current limits on Z', no positive signature is expected in the future DM-electron experiments. The most promising scenario was $m_{Z'} \approx 2$ TeV with $m_\chi/m_{Z'} \simeq 0.4$, which would lead to observable signatures in the direct, indirect, and collider experiments. Increasing the mass ratio $m_\chi/m_{Z'}$ made it easier for the model to escape current limits, but it also became harder to detect in dark matter experiments. Meanwhile, various experiments have been proposed to test the new gauge boson Z', which covers the most viable parameter space of the dark matter in the future.

ACKNOWLEDGMENTS

This work is supported by the National Natural Science Foundation of China under Grant No. 11805081, the Natural Science Foundation of Shandong Province under Grants No. ZR2022MA056 and No. ZR2024QA138, the Open Project of Guangxi Key Laboratory of Nuclear Physics and Nuclear Technology under Grant No. NLK2021-07, and the University of Jinan Disciplinary Cross-Convergence Construction Project 2024 (XKJC-202404).

DATA AVAILABILITY

No data were created or analyzed in this study.

[1] M. Cirelli, A. Strumia, and J. Zupan, arXiv:2406.01705.
[2] L. Roszkowski, E. M. Sessolo, and S. Trojanowski, Rep. Prog. Phys. **81**, 066201 (2018).
[3] G. Arcadi, M. Dutra, P. Ghosh, M. Lindner, Y. Mambrini, M. Pierre, S. Profumo, and F. S. Queiroz, Eur. Phys. J. C **78**, 203 (2018).
[4] G. Arcadi, D. Cabo-Almeida, M. Dutra, P. Ghosh, M. Lindner, Y. Mambrini, J. P. Neto, M. Pierre, S. Profumo, and F. S. Queiroz, Eur. Phys. J. C **85**, 152 (2025).
[5] P. J. Fox and E. Poppitz, Phys. Rev. D **79**, 083528 (2009).
[6] T. Cohen and K. M. Zurek, Phys. Rev. Lett. **104**, 101301 (2010).
[7] Y. Bai and J. Berger, J. High Energy Phys. 08 (2014) 153.
[8] S. Chang, R. Edezhath, J. Hutchinson, and M. Luty, Phys. Rev. D **90**, 015011 (2014).
[9] B. Abi *et al.* (Muon g-2 Collaboration), Phys. Rev. Lett. **126**, 141801 (2021).
[10] X. G. He, G. C. Joshi, H. Lew, and R. R. Volkas, Phys. Rev. D **43**, 22 (1991).
[11] S. Baek, N. G. Deshpande, X. G. He, and P. Ko, Phys. Rev. D **64**, 055006 (2001).
[12] M. Lindner, M. Platscher, and F. S. Queiroz, Phys. Rep. **731**, 1 (2018).
[13] S. Baek and P. Ko, J. Cosmol. Astropart. Phys. 10 (2009) 011.
[14] S. Baek, H. Okada, and K. Yagyu, J. High Energy Phys. 04 (2015) 049.
[15] S. Baek, Phys. Lett. B **756**, 1 (2016).
[16] S. Patra, S. Rao, N. Sahoo, and N. Sahu, Nucl. Phys. **B917**, 317 (2017).
[17] A. Biswas, S. Choubey, and S. Khan, J. High Energy Phys. 02 (2017) 123.
[18] A. Kamada, K. Kaneta, K. Yanagi, and H. B. Yu, J. High Energy Phys. 06 (2018) 117.

[19] X. Qi, A. Yang, W. Liu, and H. Sun, Chin. Phys. C **46**, 083102 (2022).
[20] S. Baek, J. Kim, and P. Ko, J. High Energy Phys. 01 (2025) 014.
[21] J. Wang, J. Ma, J. Gao, X. F. Han, and L. Wang, Chin. Phys. C **48**, 023101 (2024).
[22] D. Chowdhury, A. Hait, S. Mohanty, and S. Prakash, Phys. Rev. D **110**, 083023 (2024).
[23] P. Figueroa, G. Herrera, and F. Ochoa, Phys. Rev. D **110**, 095018 (2024).
[24] S. Choubey, S. Khan, M. Merchand, and S. Vihonen, J. High Energy Phys. 10 (2024) 186.
[25] P. Foldenauer, Phys. Rev. D **99**, 035007 (2019).
[26] I. Holst, D. Hooper, and G. Krnjaic, Phys. Rev. Lett. **128**, 141802 (2022).
[27] Y. M. Andreev *et al.* (NA64 Collaboration), Phys. Rev. Lett. **132**, 211803 (2024).
[28] G. Aad *et al.* (ATLAS Collaboration), J. High Energy Phys. 07 (2023) 090.
[29] G. Aad *et al.* (ATLAS Collaboration), Phys. Rev. D **110**, 072008 (2024).
[30] W. Altmannshofer, S. Gori, S. Profumo, and F. S. Queiroz, J. High Energy Phys. 12 (2016) 106.
[31] A. Biswas and A. Shaw, J. High Energy Phys. 05 (2019) 165.
[32] Z. L. Han, R. Ding, S. J. Lin, and B. Zhu, Eur. Phys. J. C **79**, 1007 (2019).
[33] R. Aaij *et al.* (LHCb Collaboration), Nat. Phys. **18**, 277 (2022).
[34] W. Altmannshofer and P. Stangl, Eur. Phys. J. C **81**, 952 (2021).
[35] J. P. Delahaye, M. Diemoz, K. Long, B. Mansoulié, N. Pastrone, L. Rivkin, D. Schulte, A. Skrinsky, and A. Wulzer, arXiv:1901.06150.
[36] C. Accettura, D. Adams, R. Agarwal, C. Ahdida, C. Aimè, N. Amapane, D. Amorim, P. Andreetto, F. Anulli, R. Appleby *et al.*, Eur. Phys. J. C **83**, 864 (2023); **84**, 36(E) (2024).
[37] G. y. Huang, F. S. Queiroz, and W. Rodejohann, Phys. Rev. D **103**, 095005 (2021).
[38] A. Dasgupta, P. S. B. Dev, T. Han, R. Padhan, S. Wang, and K. Xie, J. High Energy Phys. 12 (2023) 011.
[39] J. Sun, F. Huang, and X. G. He, Phys. Lett. B **845**, 138121 (2023).
[40] K. Korshynska, M. Löschner, M. Marinichenko, K. Mekała, and J. Reuter, Eur. Phys. J. C **84**, 568 (2024).
[41] B. De, Eur. Phys. J. C **85**, 81 (2025).
[42] G. Krnjaic, G. Marques-Tavares, D. Redigolo, and K. Tobioka, Phys. Rev. Lett. **124**, 041802 (2020).
[43] N. Okada and O. Seto, Phys. Rev. D **101**, 023522 (2020).
[44] K. Asai, S. Okawa, and K. Tsumura, J. High Energy Phys. 03 (2021) 047.
[45] M. Drees and W. Zhao, Phys. Lett. B **827**, 136948 (2022).
[46] T. Hapitas, D. Tuckler, and Y. Zhang, Phys. Rev. D **105**, 016014 (2022).
[47] K. Deka, S. Sadhukhan, and M. P. Singh, arXiv:2203.17122.
[48] M. Escudero, D. Hooper, G. Krnjaic, and M. Pierre, J. High Energy Phys. 03 (2019) 071.
[49] M. Bauer, P. Foldenauer, and J. Jaeckel, J. High Energy Phys. 07 (2018) 094.
[50] N. Aghanim *et al.* (Planck Collaboration), Astron. Astrophys. **641**, A6 (2020); **652**, C4(E) (2021).
[51] K. Akita and M. Yamaguchi, J. Cosmol. Astropart. Phys. 08 (2020) 012.
[52] J. Froustey, C. Pitrou, and M. C. Volpe, J. Cosmol. Astropart. Phys. 12 (2020) 015.
[53] P. Foldenauer and J. Hoefken Zink, J. High Energy Phys. 07 (2024) 096.
[54] J. P. Lees *et al.* (*BABAR* Collaboration), Phys. Rev. D **94**, 011102 (2016).
[55] W. Altmannshofer, S. Gori, M. Pospelov, and I. Yavin, Phys. Rev. Lett. **113**, 091801 (2014).
[56] S. Alekhin, W. Altmannshofer, T. Asaka, B. Batell, F. Bezrukov, K. Bondarenko, A. Boyarsky, K. Y. Choi, C. Corral, N. Craig *et al.*, Rep. Prog. Phys. **79**, 124201 (2016).
[57] A. Berlin, N. Blinov, G. Krnjaic, P. Schuster, and N. Toro, Phys. Rev. D **99**, 075001 (2019).
[58] H. Davoudiasl, H. Liu, R. Marcarelli, Y. Soreq, and S. Trifinopoulos, J. High Energy Phys. 03 (2025) 046.
[59] C. Cesarotti and R. Gambhir, J. High Energy Phys. 05 (2024) 283.
[60] S. Airen, E. Broadberry, G. Marques-Tavares, and L. Ricci, arXiv:2412.09681.
[61] S. Gninenko and D. Gorbunov, Phys. Lett. B **823**, 136739 (2021).
[62] S. R. Mishra *et al.* (CCFR Collaboration), Phys. Rev. Lett. **66**, 3117 (1991).
[63] S. N. Gninenko, N. V. Krasnikov, and V. A. Matveev, Phys. Rev. D **91**, 095015 (2015).
[64] I. Adachi *et al.* (Belle-II Collaboration), Phys. Rev. D **109**, 112015 (2024).
[65] A. K. Barik, S. K. Rai, and A. Srivastava, arXiv:2408.14396.
[66] K. Griest and D. Seckel, Phys. Rev. D **43**, 3191 (1991).
[67] G. Belanger, F. Boudjema, A. Pukhov, and A. Semenov, Comput. Phys. Commun. **185**, 960 (2014).
[68] A. H. Abdelhameed *et al.* (CRESST Collaboration), Phys. Rev. D **100**, 102002 (2019).
[69] P. Agnes *et al.* (DarkSide-50 Collaboration), Phys. Rev. D **107**, 063001 (2023).
[70] E. Aprile *et al.* (XENON Collaboration), Phys. Rev. Lett. **131**, 041003 (2023).
[71] F. Acerbi *et al.* (DarkSide-20k Collaboration), Commun. Phys. **7**, 422 (2024).
[72] J. Aalbers *et al.* (DARWIN Collaboration), J. Cosmol. Astropart. Phys. 11 (2016) 017.
[73] C. A. J. O'Hare, Phys. Rev. Lett. **127**, 251802 (2021).
[74] J. Aalbers *et al.* (LZ Collaboration), arXiv:2410.17036.
[75] L. Barak *et al.* (SENSEI Collaboration), Phys. Rev. Lett. **125**, 171802 (2020).
[76] I. M. Bloch *et al.* (SENSEI Collaboration), Phys. Rev. Lett. **134**, 161002 (2025).
[77] C. Cheng *et al.* (PandaX-II Collaboration), Phys. Rev. Lett. **126**, 211803 (2021).
[78] E. Aprile *et al.* (XENON Collaboration), Phys. Rev. Lett. **123**, 251801 (2019).
[79] M. Battaglieri, A. Belloni, A. Chou, P. Cushman, B. Echenard, R. Essig, J. Estrada, J. L. Feng, B. Flaugher, P. J. Fox *et al.*, arXiv:1707.04591.

[80] C. A. Argüelles, A. Diaz, A. Kheirandish, A. Olivares-Del-Campo, I. Safa, and A. C. Vincent, Rev. Mod. Phys. **93**, 035007 (2021).
[81] T. Hambye, M. Hufnagel, and M. Lucca, J. Cosmol. Astropart. Phys. 05 (2022) 033.
[82] R. K. Leane, T. R. Slatyer, J. F. Beacom, and K. C. Y. Ng, Phys. Rev. D **98**, 023016 (2018).
[83] T. R. Slatyer, Phys. Rev. D **93**, 023527 (2016).
[84] K. Dutta, A. Ghosh, A. Kar, and B. Mukhopadhyaya, J. Cosmol. Astropart. Phys. 08 (2023) 071.
[85] M. Ackermann *et al.* (Fermi-LAT Collaboration), Phys. Rev. Lett. **115**, 231301 (2015).
[86] H. Abdallah *et al.* (H.E.S.S. Collaboration), Phys. Rev. Lett. **117**, 111301 (2016).
[87] M. Pierre, J. M. Siegal-Gaskins, and P. Scott, J. Cosmol. Astropart. Phys. 06 (2014) 024; 10 (2014) E01.
[88] M. Aguilar *et al.* (AMS Collaboration), Phys. Rev. Lett. **122**, 041102 (2019).
[89] A. Geringer-Sameth and S. M. Koushiappas, Phys. Rev. Lett. **107**, 241303 (2011).
[90] M. Ibe, H. Murayama, and T. T. Yanagida, Phys. Rev. D **79**, 095009 (2009).
[91] W. L. Guo and Y. L. Wu, Phys. Rev. D **79**, 055012 (2009).
[92] X. G. He, Mod. Phys. Lett. A **24**, 2139 (2009).
[93] Q. F. Xiang, X. J. Bi, S. J. Lin, and P. F. Yin, Phys. Lett. B **773**, 448 (2017).